Development of a Real-time Simulation Tool towards Self-consistent Scenario of Plasma Start-up and Sustainment on Helical Fusion Reactor FFHR-d1

Development of a Real-time Simulation Tool towards Self-consistent Scenario of Plasma Start-up and Sustainment on Helical Fusion Reactor FFHR-d1

T. Goto[1], J. Miyazawa[1], R. Sakamoto[1], Y. Suzuki[1], C. Suzuki[1], R. Seki[1], S. Satake[1], B. Huang[2], M. Nunami[1], M. Yokoyama[1], A. Sagara[1] and the FFHR Design Group[1]

[1]National Institute for Fusion Science (NIFS), Toki, Gifu, 502-5292 Japan

[2]Graduate University of Advanced Studies, Toki, Gifu, 502-5292 Japan

E-mail: goto.takuya@LHD.nifs.ac.jp

Abstract

This study closely investigates the plasma operation scenario for the LHD-type helical reactor FFHR-d1 in view of MHD equilibrium/stability, neoclassical transport, alpha energy loss and impurity effect. In 1D calculation code that reproduces the typical pellet discharges in LHD experiments, we identify a self-consistent solution of the plasma operation scenario which achieves steady-state sustainment of the burning plasma with a fusion gain of $Q \sim 10$ was found within the operation regime that has been already confirmed in LHD experiment. The developed calculation tool enables systematic analysis of the operation regime in real time.

Keywords: heliotron, reactor design, plasma start-up scenario, MHD, neoclassical transport, bootstrap current

1. Introduction

Helical systems with a net current-free plasma are inherently advantageous in steady-state operation: no disruptive event due to plasma current, high plant efficiency because of no need of current drive power. Among various helical systems, heliotron systems with two continuous helical coils, represented by the Large Helical Device (LHD), have achieved remarkable steady-state plasma performance with a highly reliable operating system [1]. Based on the LHD achievements, conceptual design of the LHD-type helical reactor FFHR-d1 with a major radius 4 times that of LHD ($R_c = 15.6$ m) has been advanced by utilizing the knowledge gained from past design studies and the engineering R&D of large-size superconducting devices including ITER [2]. In the previous study [3], the plasma operation control scenario of FFHR-d1 towards a steady-state self-ignition operation point has been examined by 1D calculation code based on LHD experimental observations and detailed physics analysis tools provided in the integrated transport analysis suite TASK3D [4]. In this previous study, the MHD equilibrium and the power balance between the total absorbed power and the neoclassical energy loss has been examined. It was found that start-up and steady-state sustainment of self-ignition plasma with a fusion power of 3 GW is achievable in the case of the design option of FFHR-d1 with high magnetic field (hereafter this option is called as FFHR-d1B): the magnetic field strength at the helical coil winding centre B_c is 5.6 T.

However, compatibility between MHD stability and good energy confinement is recognized as one of the big issues of the heliotron system. The effect of bootstrap current on the plasma burning conditions has not been fully examined. In this study, these issues (i.e., MHD stability, anomalous transport and bootstrap current) are addressed by extending the 1D calculation code and plasma operation regime of FFHR-d1B was examined in depth. Section 2 briefly reviews the calculation model and states the prerequisites of the calculation are given in Section 2. The calculation results are given in Section 3. Finally, these are summarized in Section 4.

2. Calculation method

2.1. 1D Calculation model

In LHD experiments, gryo-Bohm type parameter dependence has been widely observed not only in global energy confinement property but also local relationship between the electron pressure and density: $p_e(r) \propto n_e(r)^{0.6}$[5]. Based on this fact, Sakamoto et al. [6] developed a simplified model for analysing the pellet fuelling requirements. In this model, time evolution of the electron density n_e is calculated by solving the following 1D diffusion equation in cylindrical geometry:

$$\frac{\partial n_e}{\partial t} = \frac{1}{r}\frac{\partial}{\partial r}\left\{ r\left(D\frac{\partial n_e}{\partial r} - n_e V \right) \right\} + S . \qquad (1)$$

According to the experimental observation of typical pellet-fuelled LHD discharges, no advection flow ($V = 0$) and the spatially constant diffusion coefficient

$$D(r) = D \propto \left(P_{abs}/\overline{n}_e \right)^{0.6} B_{ax}^{-0.8} \qquad (2)$$

are assumed, where P_{abs}, $\overline{n}_e$ and B_{ax} are the total absorbed power, the line-averaged electron density and the magnetic field strength at the magnetic axis, respectively. Time evolution of the electron temperature is calculated from that of the electron pressure. Considering the above-mentioned gyro-Bohm-type parameter dependence, the time evolution of the electron pressure is estimated as follows:

$$\frac{\partial p_e(r)}{\partial t} = \frac{1}{\tau_E}\left(\gamma_{DPE*}\hat{p}_e(r)a^{2.4}R^{0.6}P_{abs}^{0.4}B^{0.8}n_e(r)^{0.6} - p_e(r) \right), \qquad (3)$$

where τ_E, a and R are the energy confinement time, average plasma minor radius and plasma major radius, respectively. The energy confinement time is calculated as

$$\tau_E = \frac{W_p}{P_{abs}}, \qquad (4)$$

where W_p is plasma stored energy. γ_{DPE*} is the confinement improvement factor estimated from the heating profile [7]:

$$\gamma_{DPE*} = \left\{ \frac{1 - 0.35/C_{aux}}{\left(P_{dep}/P_{dep1} \right)_{avg}} \right\}^{0.6}, \qquad (5)$$

$$C_{aux} = \frac{P_{abs}}{P_{abs} - P_{aux}}, \qquad (6)$$

$$P_{dep}(r) = \int_0^r P_{dep}(r')\left(\frac{dV}{dr'} \right)dr', \qquad (7)$$

$$\left(P_{dep}/P_{dep1} \right)_{avg} = \int_0^1 \frac{P_{dep}(r)}{P_{dep}(1)}dr, \qquad (8)$$

where $P_{dep}(r)$ and P_{aux} are the heat deposition profile and the auxiliary heating power, respectively. $\hat{p}_e(r)$ is the gyro-Bohm normalized electron pressure of the reference LHD experimental data:
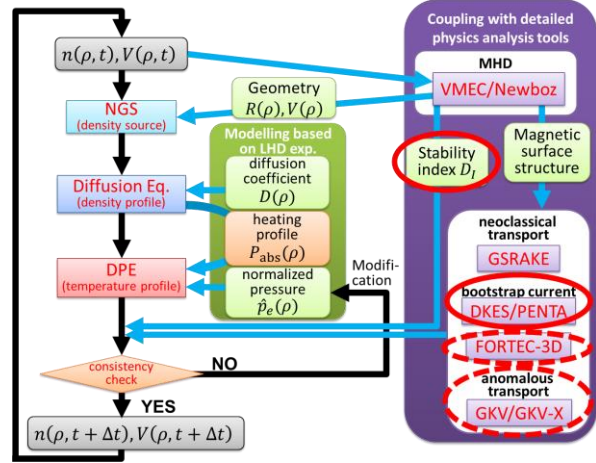
$$\hat{p}_e(r) = \frac{p_{e,exp}(r)}{a_{exp}^{2.4}R_{exp}^{0.5}P_{abs,exp}^{0.4}B_{exp}^{0.8}n_{e,exp}(r)^{0.6}} . \qquad (9)$$

In Eq. (9), the subscript 'exp' denotes that the parameters are obtained from the reference experimental data. In this model, the plasma charge neutrality, temperature equality ($T_e = T_i$) and diffusion coefficient of ions equal to that of electrons are assumed. Considering the fuelling by pellet injection, the particle source term S in Eq. (1) was assigned as the ablation profile of the pellet calculated by the Neutral Gas Shielding (NGS) model [8]. At the timing of the pellet ablation, electron density and temperature are assumed to change adiabatically.
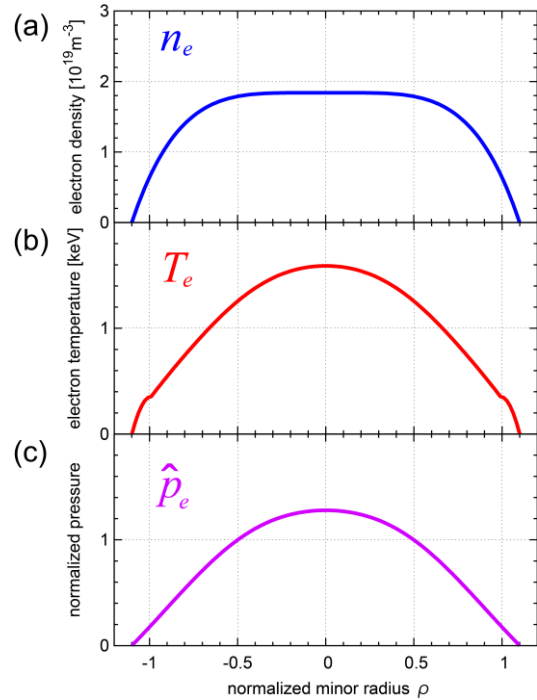
This reduced model reproduces the waveform of the electron density, the electron temperature and the plasma stored energy of the typical pellet discharges in LHD experiments, for example, $n_e \sim 1.5 \times 10^{20}$ m^{-3}, $T_e \sim 2$ keV and heating power of ~ 14 MW, respectively [9]. However, this model is an 'abductive' inference and does not consider the consistency with MHD equilibrium, MHD stability, neoclassical transport, anomalous transport and bootstrap current. The MHD equilibrium, MHD stability and neoclassical transport are handled by directly coupling the calculation with detailed physics analysis tools (MHD equilibrium and stability by VMEC [10] and neoclassical transport by GSRAKE [11]). The models and scalings provided by these tools were also used. Similar techniques are being developed for anomalous transport (GKV/GKV-X [12]) and bootstrap current (DKES/PENTA [13-15] and FORTEC-3D [16]). Figure 1 is a schematic of the calculation flow.

Figure 1. Schematic of the 1D calculation. The newly implemented elements in this study are highlighted by solid circles. The modules indicated by broken circles are being developed.

2.2. Prerequisites of the calculation

In the design study of FFHR-d1, the magnetic configuration has a high plasma aspect ratio with a helical pitch parameter $\gamma_c = 1.2$ (here $\gamma_c = ma_c/(\ell R_c)$, where m, a_c and ℓ are the toroidal pitch number ($m = 10$ in this case), the minor radius of the helical coil and the number of helical coils ($\ell = 2$ in this case), respectively). This design ensures that the space between helical coil and plasma, which provides the space for the blanket modules, increases with increasing plasma aspect ratio. Regarding the radial profile of the gyro-Bohm normalized electron pressure, relatively peaked profile obtained in LHD experiment with the magnetic configuration of the inward-shifted magnetic axis position (the ratio between the magnetic axis position R_{ax} and R_c is 3.55/3.9) was selected as the reference. The gyro-Bohm normalized electron pressure profile was fitted by a single zero-order Bessel function:

Figure 2. Radial profiles of (a) electron density, (b) electron temperature, and (c) gyro-Bohm normalized electron pressure. These profiles provide the initial conditions of the calculation.

$$\hat{p}_e(\rho) = \alpha_0 J_0\left(\frac{2.4\rho}{\alpha_1}\right). \qquad (9)$$

The initial profiles are shown in Fig. 2. In the diffusion equation (Eq. (1)), the electron density at the plasma boundary (corresponding to $\rho = \alpha_1 = 1.1$ in the present case) was fixed to zero. It has been confirmed that the shape of the last closed flux surface (LCFS) can be maintained by controlling the currents if vertical field coils, which adjust the vertical magnetic field. Thus, the shape of the LCFS was fixed to that of vacuum equilibrium in MHD equilibrium calculations of VMEC. We also assume electron cyclotron heating (ECH) with frequency adjusted to the magnetic field on the axis. The power deposition profile of the auxiliary heating is the following Gaussian profile:

$$P_{aux}(\rho) = \frac{P_{aux}}{\sqrt{2\pi\sigma^2}}\exp\left(-\frac{\rho^2}{2\sigma^2}\right) \qquad (10)$$

with $\sigma = 0.05$. The power deposition profile of alpha heating was assumed as the alpha particle birth profile calculated from the radial profiles of the ion density and temperature. Considering the alpha particle orbit at the high beta operation point of FFHR-d1, calculated by MORH code, the absorption coefficient of the alpha heating power was assumed as 85%[17]. Although this calculation does not explicitly compute the ion thermal transport, the helium impurity effect is reflected through the dilution effect and the effective charge in the calculated Bremsstrahlung power loss. No other impurity was considered in the calculation. In the GSRAKE, DKES/PENTA and FORTEC-3D calculations, we assumed pure deuterium plasma and self-consistently solved ambipolar radial electric field so that the ion and electron fluxes were equalized on every flux surfaces. The pellet fuelling assumed a fixed size pellet (containing 2×10^{22} particles) injected at 1.5 km/s, which requires no special technological development. Considering the time resolution of the density measurement, the minimum injection interval was set to 5 ms.

3. Calculation result

The plasma operation regime of FFHR-d1B ($R_c = 15.6$ m, $a_c = 3.744$ m and $B_c = 5.6$ T) was examined in the developed 1D simulation code. In LHD experiments, the plasma operation regime is limited mainly by the MHD instability and edge density. Regarding the former condition, a low-n MHD mode that causes collapse of the core pressure emerges when the Mercier index D_I [18] at $m/n = 1$ rational surface (corresponding to the radial position with $\iota/2\pi = 1$) exceeds 0.2–0.3. Regarding the latter condition, radiation collapse occurs when the edge electron density exceeds the Sudo density limit [19]. Moreover, the transport loss is 2–3 times larger in typical LHD plasma than in the theoretically-predicted neoclassical transport loss [20]. The
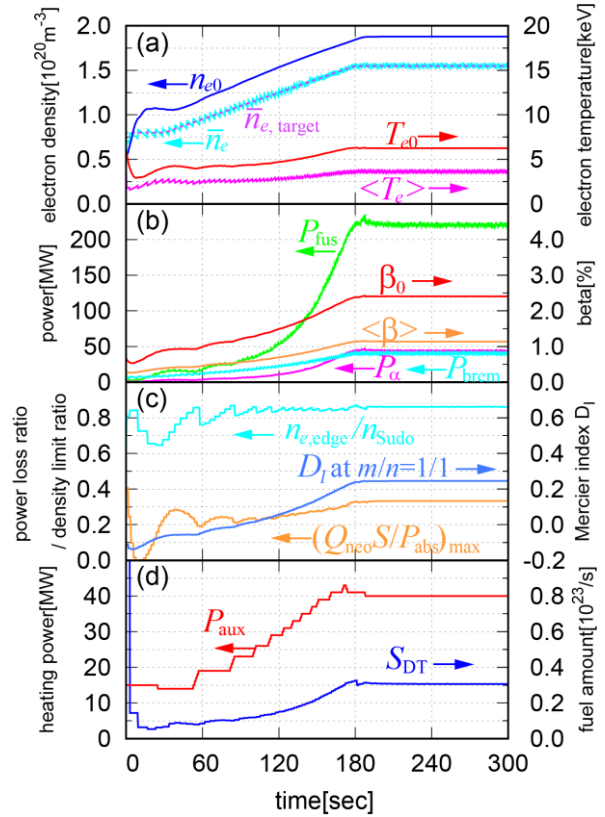
Figure 3. Time evolution of (a) electron density and temperature, (b) fusion power, alpha power, bremsstrahlung loss and beta value, (c) ratio of neoclassical energy loss to the total absorbed power, ratio of the edge electron density to Sudo density limit and Mercier index and (d) external heating power and the injected fuel amount in the $Q \sim 5$ operation of FFHR-d1.

dependence of the operation regime on these critical physics parameters was analysed in this study.

The pellet fuelling and external heating were controlled by a method developed in the previous study [2], which requires only a small number of simple diagnostics. The injection timing of the pellet was determined by PID control based on the line-averaged electron density. The external heating power was increased when the edge electron density (at $\rho = 1.0$) exceeded the pre-set value (based on the Sudo density limit but with several margins), and decreased when the fusion power exceeded its target value. The range and time interval of the minimum variation in the external heating power were set to 1 MW and 1 sec, respectively.

Figure 3 shows the time evolution of the plasma and the externally controlled parameters including the above-mentioned critical physics parameters (Mercier index and ratio of neoclassical energy loss to the total absorbed power). Here we conservatively ensured $D_I < 0.25$ at $\iota/2\pi = 1$ and set the energy loss by neoclassical transport to one-third of the volume-integrated total absorbed power at any radial position. Under these conditions, the energy loss by anomalous transport can be twice of neoclassical transport. Consequently, a steady-state, sub-ignition operation with a fusion power of ~ 200 MW and an external heating power of ~ 40 MW (i.e. fusion gain Q ~5) was attained. Figure 4 shows the electron density and temperature profiles at the steady-state operation point (t = 300 s in Fig. 2).

Figure 5 shows the radial profiles of the Mercier index D_I and rotational transform $\iota/2\pi$, and Figure 6 shows the radial profiles of the neoclassical energy flux and the volume-integrated total absorbed power. The plasma operation contour (POPCON) plot at this steady-state operation point is shown in Fig. 7. Although the final operation point locates in the thermally unstable region (left of the saddle point), the electron temperature is restrained by the increased neoclassical energy loss, so steady state is achieved.

As shown in Fig. 4, the electron density profile of the burning plasma flattens due to the shallow pellet penetration. The shoulder in the radial profile indicated the location of the front of the pellet ablation profile locates. Because this ablation profile is a function of the electron density
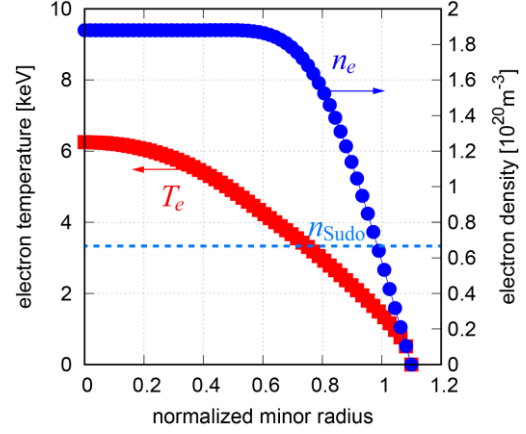
Figure 4. Radial profiles of the electron density (circles) and electron temperature (squares) at the steady-state operation point with Q ~ 5. The Sudo density limit is also plotted (broken line).
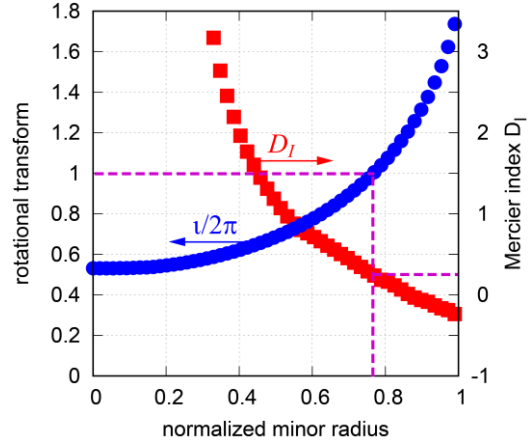

Figure 5. Radial profiles of the Mercier index (squares) and rotational transform (circles) at the steady-state operation point with Q ~ 5.
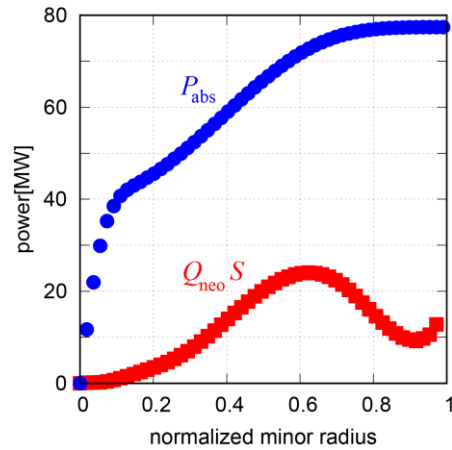

Figure 6. Radial profiles of the neoclassical energy flux (squares) and the volume-integrated total absorbed power (circles) at the steady-state operation point with Q ~ 5.

and temperature profiles and the normalized electron pressure profile is assumed fixed, the density profile is uniquely determined if the electron density and temperature at the core ($\rho = 0$) are given. Thus, we can plot the contours of the Mercier index and the ratio of neoclassical energy loss to the total absorbed power in a POPCON plot (see Fig. 7). The plot quantified the conditions of amplified fusion gain. For example, relaxing the restriction on the neoclassical transport is more effective than relaxing that on the Mercier index to increase the fusion gain to around 10. Figure 8 shows the time evolution of the plasma and externally controlled parameters under slightly relaxed conditions from the previous case, but within the parameter range confirmed in the LHD experiment. Here, $D_I < 0.3$ at $\iota/2\pi = 1$ and the energy loss by neoclassical transport is one-half the total absorbed power, meaning that the energy loss by anomalous transport is suppressed to the same as the loss by the neoclassical transport. The design achieved steady-state operation with $Q > 10$ (fusion power of ~ 400 MW under an external heating power of ~ 35 MW). Figure 9 shows the radial profiles of the electron density and temperature at this $Q \sim 10$ operation point. The density is lower and the temperature is higher than in the case of $Q \sim 5$. Radial profiles of the integrated total neoclassical energy flux and the volume-integrated total absorbed power are shown in Fig. 10.

The bootstrap current was also analysed at the $Q \sim 10$ operation point. Figures 11 and 12 show the profiles of the rotational transform and bootstrap current density, respectively, where the bootstrap current was estimated by PENTA code. In neoclassical transport theory, the momentum conservation property of Coulomb collisions is essential for evaluating the bootstrap current. The momentum correction technique in the PENTA code has been recently verified by a delta-f Monte Carlo code [21]. The calculation was iterated because the bootstrap current alters the equilibrium. The shape of the LCFS was assumed constant. The calculation converged after 3 iterations and the total toroidal bootstrap current was estimated as 0.55 MA. As shown in Fig. 11, the rotational transform slightly
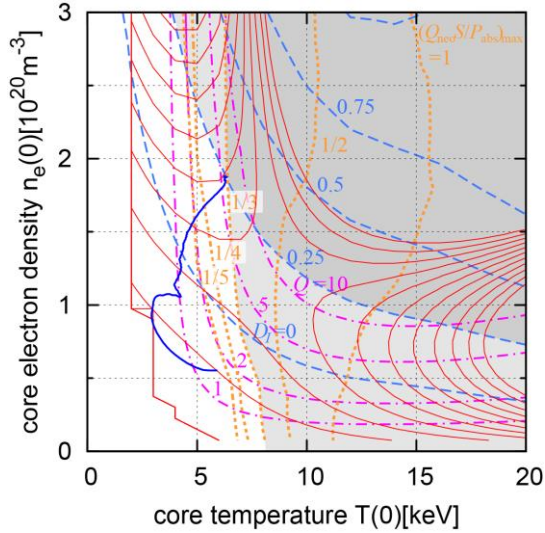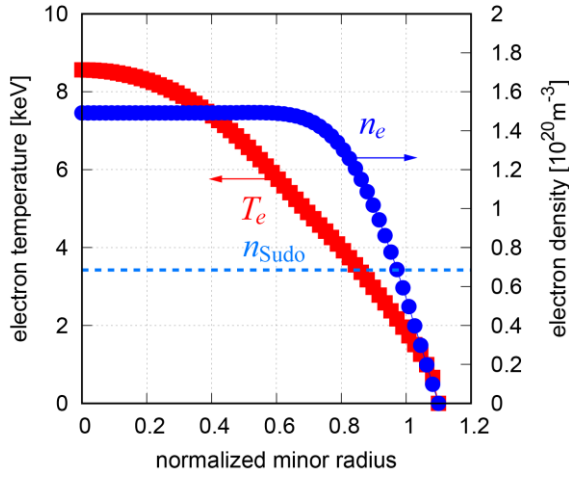

Figure 7. POPCON plot at the steady-state operation point with a fusion gain of $Q \sim 5$. Thin solid curves are the contours of the external heating power required to sustain the plasma. The interval of the contour lines is 10 MW. Thick solid curve is the trajectory of the electron density and temperature. Contours of the fusion gain (dashed-dotted line), the Mercier index (broken line) and the ratio of the neoclassical energy loss to the total absorbed power (dotted line) are also plotted. The shaded region corresponds to the operation regime that violates the conditions of the present calculation.
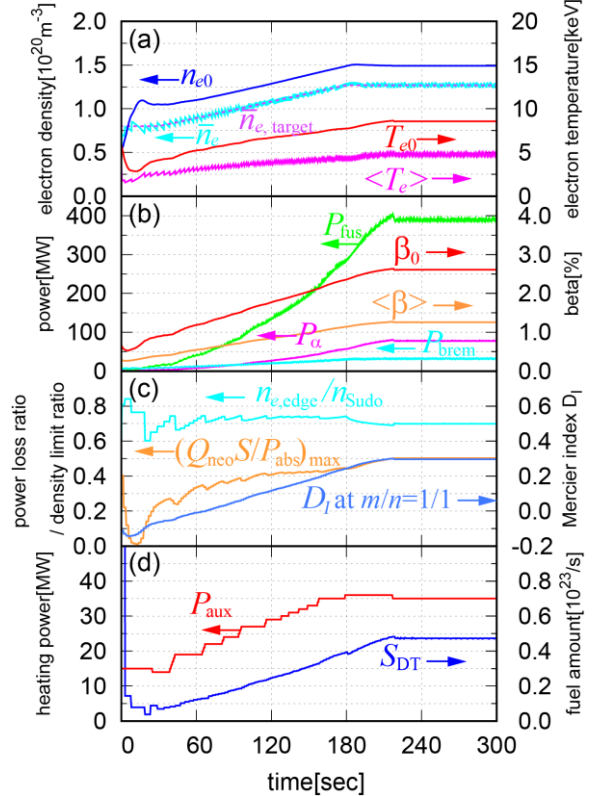

Figure 8. Time evolutions of plasma and the externally controlled parameters in the FFHR-d1 operating at $Q \sim 10$. The parameters are described in the caption of Fig. 3.

increased over the entire region. However, the changes were slight, implying that the estimated bootstrap current would not change the MHD phenomena and hence overturn the present results.

It should be emphasized that further increase in the fusion gain is expected. By simultaneously relaxing the constraints of MHD stability and transport loss by means of the configuration optimization, the operation regime would drastically expand towards the region of high fusion gain. Confinement improvement or engineering design optimisation (e.g., increasing the magnetic field by optimising the coil design) would also increase the fusion gain, because less external heating power would be required to sustain plasma with the same beta value. Therefore, deuterium experiments of the LHD and design optimisation studies of FFHR are strongly expected to improve the operation scenario of FFHR-d1B.


Figure 9. Radial profiles of electron density (circles) and electron temperature (squares) at the steady-state operation point with $Q \sim 10$. The Sudo density limit is also plotted (broken line).
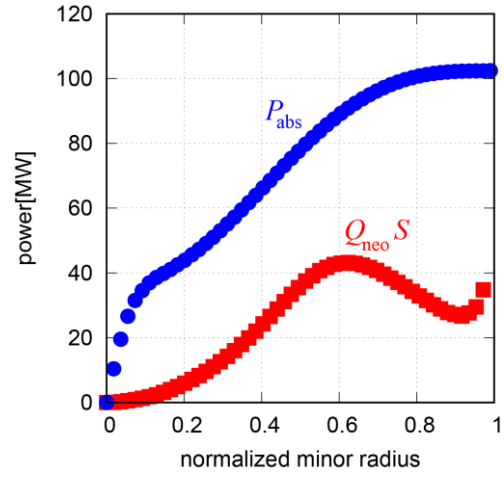
Figure 10. Radial profiles of the neoclassical energy flux (squares) and volume-integrated total absorbed power (circles) at the steady-state operation point with $Q \sim 10$.
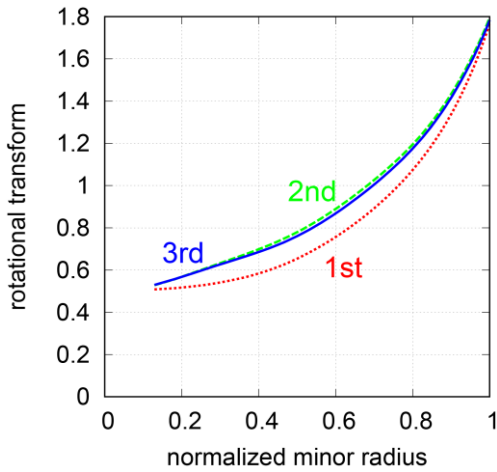
Figure 11. Radial profile of rotational transform at the steady-state operation point with $Q \sim 10$ and a 0.55 MA bootstrap current. Dotted, broken and solid lines plot the initial, second and third (converged) calculation results, respectively.
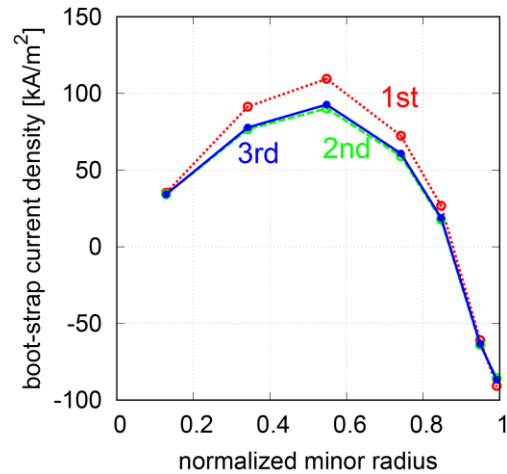
Figure 12. Radial profiles of the bootstrap current density at the steady-state operation point with $Q \sim 10$. Dotted, broken and solid lines represent the initial, second and third (converged) calculation results, respectively.

4. Summary

The plasma operation regime of the LHD-type helical fusion reactor FFHR-d1B was closely examined by coupling 1D simulation code with detailed physics analysis tools. The results confirmed that steady-state operation with a fusion gain of $Q > 10$ is possible in a self-consistent plasma operation regime in view of MHD equilibrium, MHD stability, neoclassical transport, density limit, helium impurity fraction, alpha energy loss and bootstrap current. The effects of the plasma and engineering design parameters on the operation regime were quantified. Although further detailed analysis including temperature inequality, effect of the edge neutral particles and the deposition profile of the heating power is needed, the present study provides the design direction and the physics and engineering R&D issues of LHD-type helical reactors. The design requirements for the proper control of the plasma operation were identified, and the study contributes to the overall plant system design. The developed calculation tool will guide the development of a real-time predictive simulation tool of the core plasma which will aid the plasma operation control of future fusion power plants.

Acknowledgements

References

[1]   Komori A. *et al* 2010 *Fusion Sci. Technol.* **58** 1
[2]   Sagara A. *et al* 2012 *Fusion Eng. Des.* **87** 594
[3]   Goto T. *et al* 2015 *Nucl. Fusion* **55** 063040
[4]   Yokoyama M. *et al* 2013 *Plasma Fusion Res.* **8** 2403016
[5]   Miyazawa J. *et al* 2012 *Nucl. Fusion* **52** 123007
[6]   Sakamoto R. *et al* 2012 *Nucl. Fusion* **52** 083006
[7]   Miyazawa J. *et al* 2014 *Nucl. Fusion* **54** 013014
[8]   Parks P.B. *et al* 1978 *Phys. Fluids* **21** 1735
[9]   Sakamoto R. *et al* 2015 *Proc. of 26th Symposium on Fusion Engineering*, USA, SO15-2
[10] Hirshman S.P. *et al* 1983 *Phys. Fluids* **26** 3553
[11] Beidler C.D. *et al* 1995 *Plasma Phys. Control. Fusion* **37** 463
[12] Nunami M. *et al* 2010 *Plasma Fusion Res.* **5** 016
[13] Hirshman S.P. *et al* 1986 *Phys. Fluids* **29** 2951
[14] Spong D.A. *et al* 2005 *Phys. Plasmas* **12** 056144
[15] Sugama H. *et al* 2002 *Phys. Plasmas* **9** 4637
[16] Satake S. *et al* 2008 *Plasma Fusion Res.* **3** S1062
[17] Miyazawa J. *et al* 2014 *Nucl. Fusion* **54** 043010
[18] Glasser A. H. *et al* 1975 *Phys. Fluids* **18** 875
[19] Miyazawa J *et al* 2010 *Fusion Sci. Technol.* **58** 200
[20] Yamada H *et al* 2010 *Phys. Rev. Lett.* **84** 1216
[21] Huang B *et al* 2017 *Plasma Fusion Res.* **12** 1203004